analytical chemistry

Article

Cite This: Anal. Chem. 2019, 91, 12181−12190

pubs.acs.org/ac

Ultrasensitive, Selective, and Highly Stable Bioelectronic Nose That Detects the Liquid and Gaseous Cadaverine

Jungkyun Oh,[†,‡] Heehong Yang,[†,‡,§] Go Een Jeong,[†] Dongseok Moon,[†] Oh Seok Kwon,[∥] Sooyeol Phyo,[⊥] Jiwon Lee,[⊥] Hyun Seok Song,[*,#,○] Tai Hyun Park,[*,†] and Jyongsik Jang[*,†]

[†]School of Chemical and Biological Engineering, Institute of Chemical Processes, Seoul National University, Seoul 08826, Republic of Korea

[∥]Infectious Disease Research Center, Korea Research Institute of Bioscience and Biotechnology (KRIBB), Daejeon 34141, Republic of Korea

[⊥]Center for Environment, Health and Welfare Research, Korea Institute of Science and Technology, Seoul 02792, Republic of Korea

[#]Sensor System Research Center, Korea Institute of Science and Technology, Seoul 02792, Republic of Korea

[○]Division of Bioconvergence Analysis, Korea Basic Science Institute (KBSI), Cheongju 28119, Republic of Korea

Supporting Information

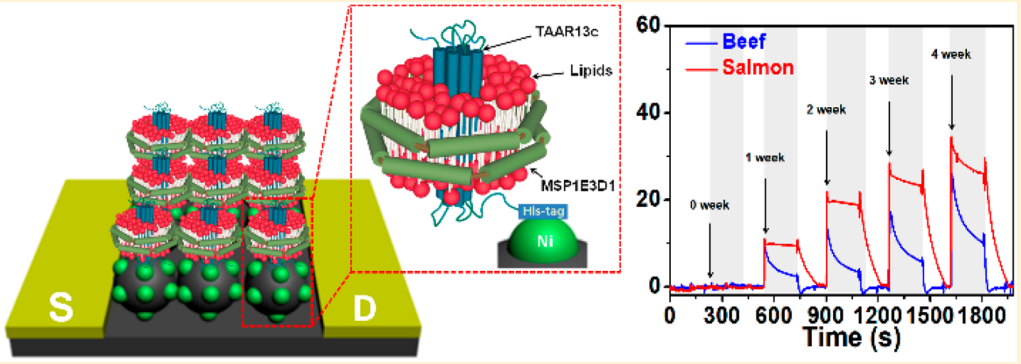

ABSTRACT: Field-effect transistor (FET) devices based on conductive nanomaterials have been used to develop biosensors. However, development of FET-based biosensors that allow efficient stability, especially in the gas phase, for obtaining reliable and reproducible responses remains a challenge. In this study, we developed a nanodisc (ND)-functionalized bioelectronic nose (NBN) based on a nickel (Ni)-decorated carboxylated polypyrrole nanoparticle (cPPyNP)-FET that offers the detection of liquid and gaseous cadaverine (CV). The TAAR13c, specifically binding to CV, which is an indicator of food spoilage, was successfully constructed in NDs. The NBN was fabricated by the oriented assembly of TAAR13c-embedded NDs (T13NDs) onto the transistor with Ni/cPPyNPs. The NBN showed high performance in selectivity and sensitivity for the detection of CV, with excellent stability in both aqueous and gas phases. Moreover, the NBN allowed efficient measurement of corrupted real-food samples. It demonstrates the ND-based device can allow the practical biosensor that provides high stability in the gas phase.

Nanoelectronic sensors based on field-effect transistors (FETs) have been successfully demonstrated as highly sensitive biosensors.[1,2] Bioprobes such as antibodies,[3] antigens,[4] aptamers,[5] DNA,[6] and enzymes[7] have been widely utilized as recognition elements to enhance the selectivity of FET-based biosensors for the detection of target analytes. Even with significant advances in the development of biosensors, gas-phase sensing, which can be applied in various fields, such as the diagnosis of disease, monitoring of quality of food, and environmental analysis, has been dominated by nonbiological sensors.[8] Due to the difficulty in the retention of bioprobes with proper activities under the dry environment, the development of nanobioelectric sensors with stable bioprobes for the detection of gaseous targets, which allows reliable and rapid responses, remains challenging.[9]

Olfactory receptors (ORs) allow the identification of certain smells by recognizing odorant molecules with high specificity.[10,11] Owing to this unique property, ORs have been utilized as recognition elements for high-performance bioelectronic noses by the integration with nanomaterial-based FETs.[12−14] Moreover, the OR-based bioelectronic noses have offered the detection of target compounds in liquid phase, as well as gaseous molecules.[15,16] However, it is often difficult to achieve

Received: February 28, 2019
Accepted: September 3, 2019
Published: September 3, 2019

DOI: 10.1021/acs.analchem.9b01068
Anal. Chem. 2019, 91, 12181−12190

the construction of receptors with efficient stability on such nanostructured material surfaces, due to their complicated structures and strong hydrophobicity.[17] The function and stability of ORs as membrane proteins are highly dependent on the membrane environment, and, therefore the functional reconstitution of ORs should be an important process for the successful development of bioelectronic noses.[18] Nanovesicles derived from mammalian cells have allowed whole cell-like OR-mediated signaling with proper orientation of ORs in cell membranes and have been utilized as recognition elements for FET-based bioelectronics noses.[19−21] However, these nanovesicles have limitations in stability and reusability, and they are only functional in wet environment. It has been reported that among the various reconstitution techniques, the nanodiscs (NDs) can be the most appropriate method for the construction of receptor−nanomaterial hybrid structures.[15,18] The NDs could enable the receptor to remain in a highly stable state, even in dried condition, using lipid bilayer and membrane scaffold protein (MSP), which tightly wrap the receptor.[15] Recently, NDs incorporated with ORs produced using the *Escherichia coli* (*E. coli*) system have been successfully applied on the carbon nanotube (CNT)-based FET platform and demonstrated as the high performance bioelectronic nose.[18] However, the ND and CNT hybrid structure could not offer efficient stability for the gaseous detection.

Cadaverine (CV), a small aliphatic diamine, acts as a strong repulsive odor to human, and triggers innate behaviors in many species.[11,22] For example, Zebrafish shows avoidance response against CV, which is elicited by the highly selective sensation of CV with a particular OR, trace amine associated receptor 13c (TAAR13c).[11] The CV is often generated by the bacterial decarboxylation of amino acids, including lysine and ornithine.[11,22] Many reports have investigated the application of a specific amine sensing system to monitoring food spoilage, clinical diagnosis, and health care services.[23,24] In addition, the sensitive and selective detection of CV can be applied to various fields, such as scientific investigations and the assessment of food quality.[18]

The conducting polymer has been known that it has enormous environmental stability.[25] Thus, its characteristics could allow the biosensor based on conducting polymer to be much more stable in wet environments as well as aqueous conditions than that of other nanomaterial-based FET. The nickel (Ni)-decorated carboxylated polypyrrole nanoparticle (cPPyNP) could provide the NDs of stable immobilization with highly uniform and efficient electrostatic gating effect.[26] Moreover, the immobilization using Ni particle enables much better stability than other approaches for the sensing of analyte in the sensing phase, and quantitative analysis.[27] Furthermore, the oriented immobilization of receptor on the device enables the total number of recognition elements to be increased.[28] It has been reported that randomly oriented recognition elements may reduce the amplitude of the signal emitted after ligand binding, thus they lead to having limited capability to bind target molecules.[27]

Herein, we developed the ND-based bioelectronic nose (NBN) that allows the high-performance detection of liquid and gaseous CV with excellent stability. The TAAR13c originating from Zebrafish that has high specificity to CV was produced using the *E. coli* system, and NDs incorporated with TAAR13c (T13NDs) were successfully constructed. Ni-decorated cPPyNP-based FET platform was fabricated and conjugated with T13ND by the oriented immobilization. The NBN was set up as a liquid-ion gated FET, and could detect liquid CV with a detection limit of 100 aM, and high selectivity. For the detection of CV in the gas phase, the device offered ppb level sensitivity with high selectivity, as well as excellent stability. Furthermore, this platform allowed the efficient detection of a gaseous odor from spoiled food samples. This study should increase the capability of applying biosensors integrated with biological recognition elements in practical applications by improving stability. In addition, the NBN by this work can be used as a practical sensing tool for assessing food quality and detecting death-associated odor in scientific investigations.

EXPERIMENTAL SECTION

Reconstitution of TAAR13c Using Nanodiscs. The production process of TAAR13c and MSP using the *E. coli* system was similar to that in our previous report.[18,29] The detailed production procedure is described in the Supporting Information. Lipids (palmitoyloleoylphosphatidylcholine (POPC) and palmitoyloleoylphosphati-dylglycerol (POPG)) were mixed in chloroform at the molar ratio of 1:1. Then they were dried by nitrogen gas and put in a vacuum for 1 h to remove residual chloroform. The lipids were solubilized with the HEPES buffer I, and they were added to the purified receptor. The lipid/receptor mixture was incubated on ice for 10 min and successively mixed with MSP1E3D1. The mixed solutions were incubated with a gentle stir for 2 h at 4 °C. The final mixture contained 1 μM receptor, 8 mM lipids, 25 mM detergents, and 100 μM MSP. Afterward, Bio-Beads (Bio-Rad, U.S.A.) were added to the mixture to adsorb detergents with agitation overnight. Finally, the mixture was loaded to size exclusion chromatography (SEC; Superdex 200 Increase 10/300 GL, GE Healthcare, U.S.A.) to remove unbound units. The column was equilibrated with HEPES buffer II (20 mM HEPES-NaOH, 100 mM NaCl, and 1 mM EDTA, pH 8.0). The receptor-embedded NDs were collected, and stored at 4 °C.

Fabrication of the Receptor-Attached Ni/cPPyNP FET Sensor. The fabrication procedure for Ni/cPPy is described in the Supporting Information. To construct the FET sensor, an interdigitated microelectrode array (IDA), composed of pairs of 25 lines of gold fingers on a glass plate, was used as the immobilization substrate of Ni/cPPyNPs. An IDA electrode was treated with 5 wt % amino-silane (3-aminopropyltrimethoxysilane, APS) aqueous solution for 12 h to adopt amino groups to the electrode surface. Then, the treated electrode was exposed to 0.2 wt % Ni/cPPyNP aqueous solution (150 μL) and 1 wt % 4-(4,6-dimethoxy-1,3,5−2-yl)-4-methylmorpholinium chloride (DMT-MM) aqueous solution (150 μL) for a day. Finally, the Ni/cPPyNPs immobilized electrode was rinsed with distilled water and exposed to receptor solution, nanodisc or micelle-shaped, for 2 h at room temperature.

Gas Chromatography Analysis. The outlet of bubbler instrument and the sampling port of Tedlar bag (1 L) are linked with silicon tube and joint part of silicon tube. Each entrance was covered with Teflon tape to prevent leak of CV gas through cracks. Then, the valve of the Tedlar bag and nitrogen gas barrels, connected to bubbler, were opened to collect a CV gas sample. The nitrogen gas flows were maintained with 10 cc/min and CV gas samples with different concentrations of CV solutions were collected every 20 min. For gas chromatography (GC) analysis, the solid phase microextraction (SPME) fiber holder and assembly of 50/30

DOI: 10.1021/acs.analchem.9b01068
Anal. Chem. 2019, 91, 12181−12190

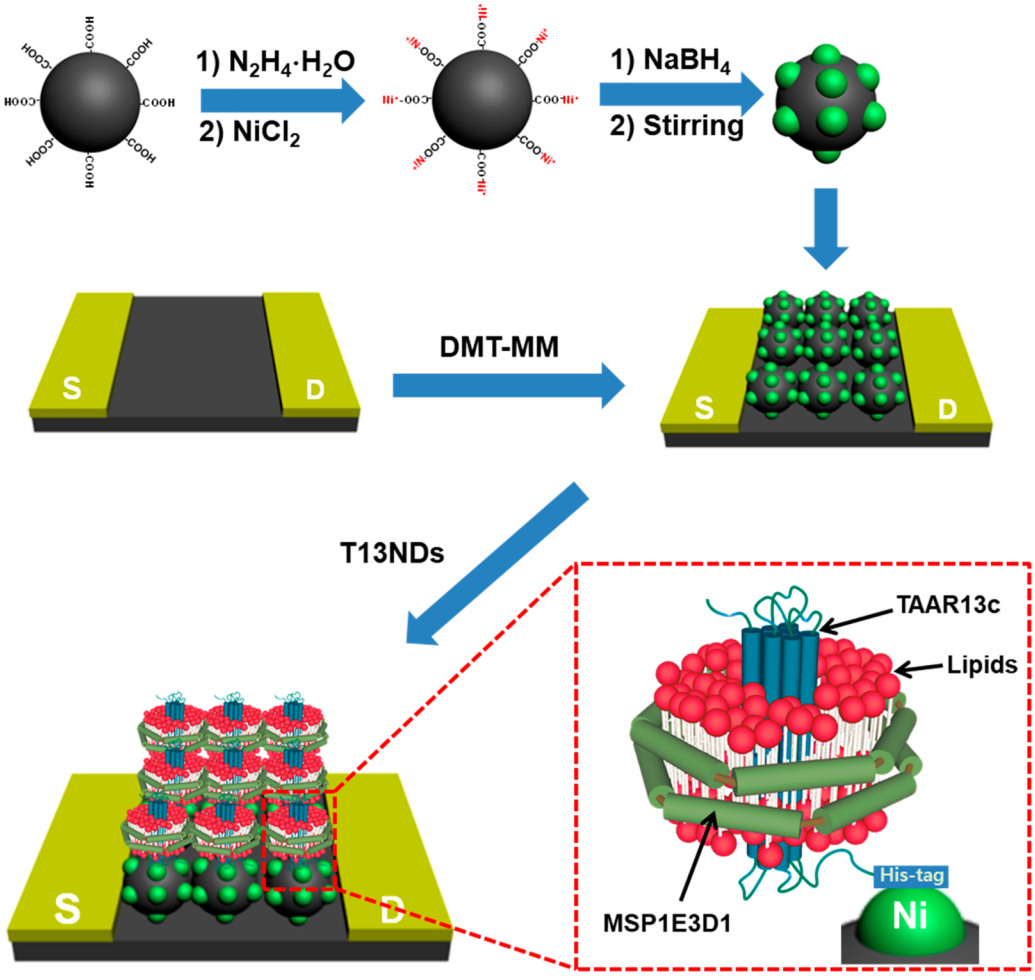

Figure 1. Schematic showing the fabrication procedure of the nanodisc-based bioelectronic nose (NBN) based on a Ni-decorated cPPyNPs sensor platform integrated with TAAR13c-embedded nanodiscs (T13NDs).

μm divinylbenzene/carboxen on polydimethylsiloxane were purchased from Supelco Inc. (Bellefonte, PA). The SPME fiber was injected and exposed into the Tedlar bag in 5 min for sampling. The fiber was then removed and inserted into the injector of a gas chromatograph 7820A (Agilent Technologies) equipped with a flame ionization detector. A total of 10 m of Rtx-5MS column (0.25 mm, thickness 0.10 μm) was used with the following temperature program: the oven was 60 °C and was held for 1 min and then increased at 10 °C/min to 80 °C. The calibration procedure was performed as follows: a 1L Tedlar bag was thoroughly cleaned by flushing the nitrogen gas. The calibration samples were prepared by transferring an aliquot of CV liquid into a Tedlar bag, diluting with nitrogen gas sequentially, and then analyzing by the same procedure for the sample from the bubbler instrument.

RESULTS AND DISCUSSION

Fabrication of the Nanodisc-Based Bioelectronic Nose. Figure 1 shows the procedure for the fabrication of NBN by the integration of Ni-decorated cPPyNP-FET and T13ND. Monodispersed cPPyNPs of ~65 nm diameter were prepared by the method in a previous work.[12,30] Briefly, cPPyNPs were fabricated by the microemulsion method, and Ni was decorated on cPPyNPs by using a chemical reduction process. A gold electrode on a glass substrate for the sensor platform was manufactured by a microelectromechanical system, including thermal evaporation and photolithograghy. Ni-decorated cPPyNPs were attached on the surface of a gold electrode by covalent bonds. For these bonds, silane treatment was progressed on the glass substrate, and 1 wt % 4-(4,6-dimethoxy-1,3,5−2-yl)-4-methylmorpholinium chloride (DMT-MM), a catalyst for bonding, was used to make the peptide bond between functional groups of silane and cPPyNP. After the fabrication process, T13NDs were conjugated on Ni-decorated cPPyNPs of the sensor platforms. T13NDs are constructed by three components, TAAR13c with His-tag at C-terminus, artificial lipids, and MSP1E3D1. The Ni^{2+} offers high affinity with a His-tag, so that the T13NDs can be immobilized on Ni/cPPyNPs with a high orientation.[15,27]

The cPPyNP with 65 nm diameter was observed by TEM instrument, Figure 2a. The cPPyNPs aqueous solution was stirred uniformly, and hydrazine monohydrate was injected to make the base condition. A $NiCl_2$ aqueous solution was added to the solution at room temperature to allow ionic interaction between the Ni^{2+} ions and the negative charges of the O atoms of the carboxylate groups in the cPPyNP structure. $NaBH_4$ powder was added to a mixed solution to reduce Ni^{2+} ions to Ni nanoparticles. The mixed solution was stirred vigorously to uniformly blend cPPyNP, Ni^{2+}, and $NaBH_4$. Figure 2b shows the transmission electron microscopy (TEM) image of Ni/cPPyNP. Ni nanoparticles of about 2−3 nm in diameter were decorated and dispersed uniformly on the surface of cPPyNP.

DOI: 10.1021/acs.analchem.9b01068
Anal. Chem. 2019, 91, 12181−12190

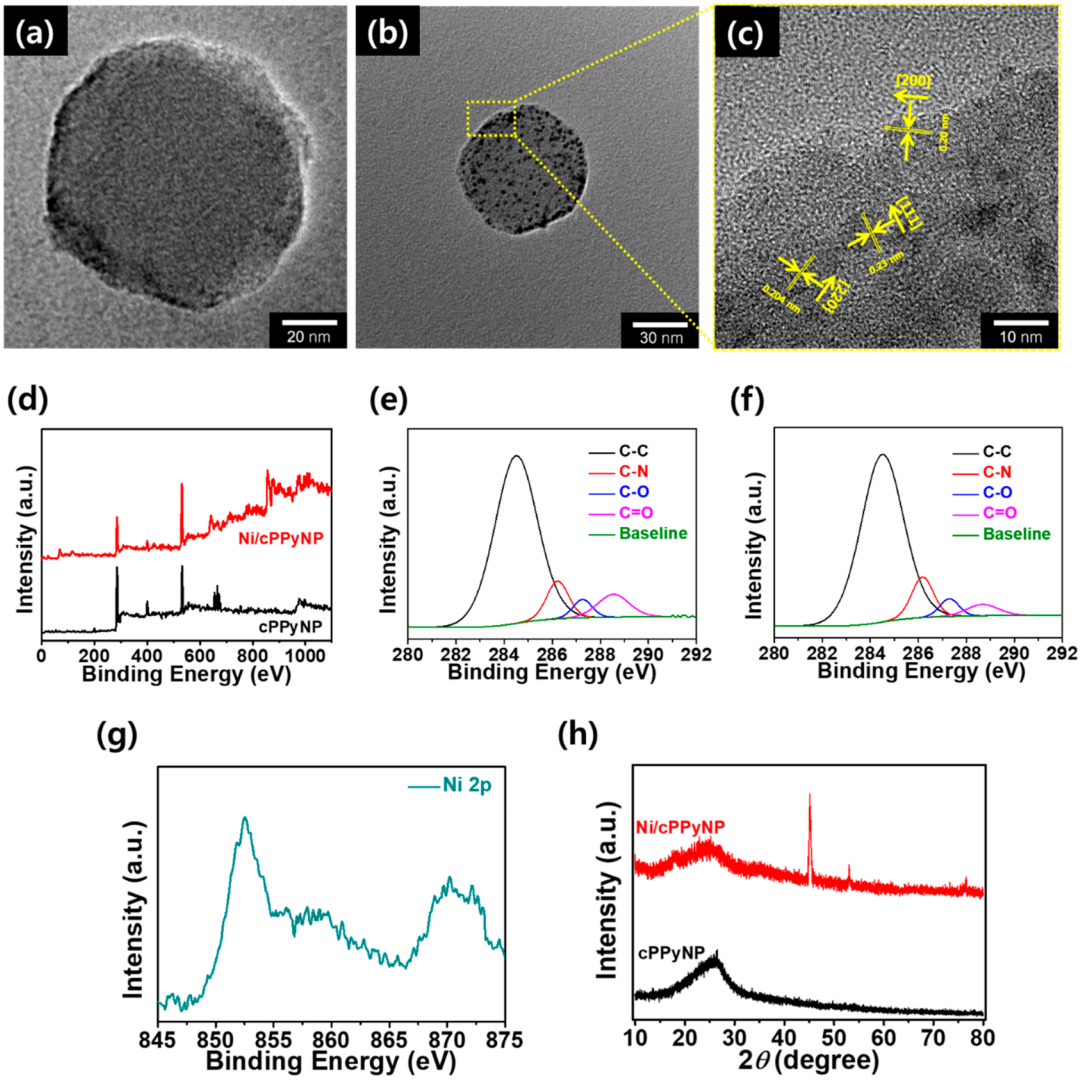

Figure 2. Characterization of Ni-decorated cPPyNPs. TEM images of (a) cPPyNP, and (b) Ni/cPPyNP, and HR-TEM image of (c) the surface of Ni/cPPyNP. X-ray photoelectron spectroscopy (XPS) spectra of (d) Ni/cPPyNP (red) and cPPyNP (black). High-resolution C 1s spectra of (e) cPPyNP, (f) Ni/cPPyNP, and (g) Ni 2P. (h) X-ray diffraction (XRD) patterns of cPPyNP (black) and Ni/cPPyNP (red).

The HR-TEM image of Ni/cPPyNP surface presents that Ni nanoparticles indicate interplanar spacings of 0.20, 0.23, and 0.204 nm for the (200), (111), and (220) planes of face centered cubic (FCC)-Ni in Figure 2c, respectively. This confirms the growth of pure crystalline Ni nanoparticles.

To further identify the composition and crystallinity of the Ni/cPPyNP, X-ray photoelectron spectroscopy (XPS) and X-ray diffraction (XRD) were used. Figure 2d displays the full spectra of XPS over the range 0−1000 eV. The XPS full spectrum of pristine cPPyNP reveals only the presence of C, N, and O atoms, while the spectrum of Ni/cPPyNP shows the presence of C, N, O, and Ni atoms. The presence of Ni peaks in the Ni/cPPyNP spectrum indicates that Ni nanoparticles had been well deposited on the surface of the cPPyNP. Figure 2e,f analyzes the high-resolution C 1s XPS peaks of cPPyNP and Ni/cPPyNP to compare the ratio of carboxyl groups of each nanoparticle. The C 1s peaks have four components. The distinguishable four peaks correspond to C−C bonds (284.6 eV), C−N bonds (286.0 eV), C−O bonds (287.5 eV), and C═O bonds (288.9 eV). The C═O bond peak of Ni/cPPyNP associated with carboxyl functional groups was decreased, rather than the C═O bond peak of cPPyNP, owing to bond breakage between C and O in the carboxyl functional groups by the chemical reduction process. Figure 2g shows the Ni 2p high-resolution spectrum of Ni/cPPyNP. Because the spin−orbit split doublet corresponds to zerovalent metallic state Ni $2p_{3/2}$ and Ni $2p_{1/2}$, two peaks with binding energy values of 852.6 and 870.0 eV show the valence state of Ni^{2+}. Figure 2h shows the X-ray diffraction (XRD) peaks of cPPyNP and Ni/cPPyNP. The broad peaks from 20° to 30° indicate the amorphous structure of cPPyNPs. The important diffraction peaks corresponding to the (111), (200), and (220) planes of nickel nanoparticle crystals (JCPDS card No. 040850) are indexed to the FCC phase Ni. This means that nickel nanoparticles were well formed on the surface of cPPyNPs.

The TAAR13c fused with His-tag was overexpressed in *E. coli* at a high level and was purified using Ni^{2+} column chromatography. Figure 3a shows the coomassie blue-stained sodium dodecyl-sulfate-polyacrylamide gel electrophoresis (SDS-PAGE) and Western blot analysis of purified TAAR13c. The clear bands at approximately 30 kDa demonstrate that TAAR13s were expressed with proper size and produced with high purity.[11,18] Although it is known that

DOI: 10.1021/acs.analchem.9b01068
Anal. Chem. 2019, 91, 12181−12190

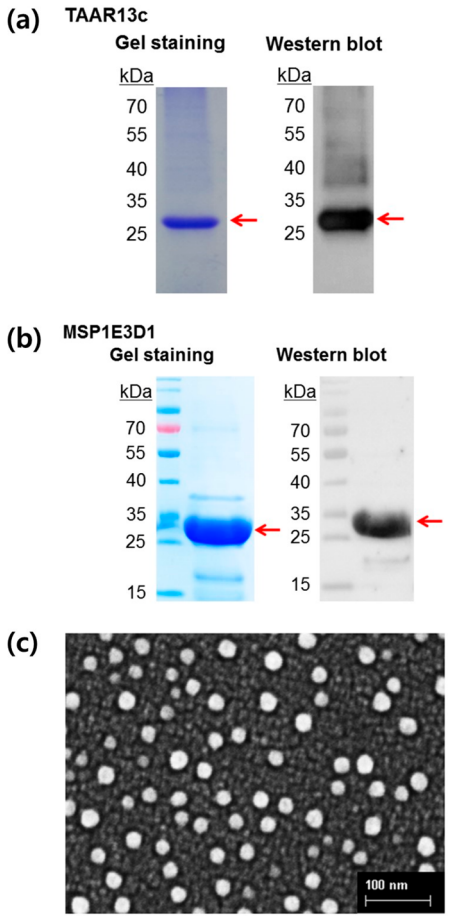

Figure 3. Production of TAAR13c-embedded nanodiscs (T13NDs). (a) SDS-PAGE and Western blot analyses of purified TAAR13c expressed in *E. coli*. (b) SDS-PAGE and Western blot analyses of MSP1E3D1 produced using *E. coli*. (c) FE-SEM image analysis of T13NDs.

the overexpression and purification of G protein-coupled receptor (GPCR) using heterologous cell systems, especially bacterial cells, is difficult,[31] the method for the production of GPCRs using the *E. coli* system has been demonstrated in our previous reports using the optimal bacterial expression vectors, including pDEST15,[32−34] pDEST17,[35] and pET-DEST42.[18,36] The MSP1E3D1 was also produced from *E. coli* as the soluble form and purified using the conventional column purification process. The purity and amount of the MSP1ED1 was confirmed by SDS-PAGE and Western blot analysis, respectively (Figure 3b). For the construction of T13NDs, TAAR13c was mixed with the detergent solution and was added to lipid−detergent mixed micelles. The MSP1E3D1 was continuously added into the mixed solution, and the T13NDs were finally obtained by the removal of detergent using Biobead. The shape and size distribution of the T13NDs was investigated by field-emission scanning electron microscopy (FE-SEM) imaging analysis (Figure 3c). The T13NDs exhibited a homogeneous discoidal shape of about 20 nm size in diameter. The homogeneity of T13NDs was further confirmed by a dynamic light scattering (DLS) measurement (Figure S1), and these results clearly demonstrate that the T13NDs were successfully self-assembled.

Detection of Cadaverine in the Liquid Phase Using the Nanodisc-Based Bioelectronic Nose. The stable state of the liquid-ion-gated FET sensor is one of the critical factors in the fabrication of sensor. The immobilization of transducer materials on the sensor electrode and T13NDs on the transducer materials was achieved to improve the stability of a FET sensor. After the fabrication of Ni/cPPyNP-FET, the solution containing T13NDs was treated on the surface of electrode to attach T13NDs on Ni/cPPyNPs. In this process, the stable immobilization was mediated by the His-tag fused at the C-terminus of the receptor, since the His-tag offers selective affinity to Ni^{2+}. To characterize the electrical properties and stability of the Ni/cPPyNPs immobilized with T13NDs (ND-Ni/cPPyNP) in the liquid phase, a liquid-ion-gate FET configuration was built using an electrolyte (Figure 4a). The sensing transducers, ND-Ni/cPPyNPs, are uniformly spread on the interdigitated electrode in the SEM image. The bright regions mean a gold array of an interdigitated electrode and dark regions mean the glass part of an electrode. Furthermore, ND-Ni/cPPyNP was confirmed by FE-SEM images in Figure 4a. The surface of Ni/cPPyNP was considerably roughened by the introduction of ND.

Figure 4b exhibits the $I_{SD}-V_{SD}$ plots of various FET electrodes at V_G = 0. These plots are used to estimate the electrical contact of the transducer materials on the electrode substrate. Each transducer material shows linearity, ohmic contact, for the voltage range of −0.1 to 0.1 V. The dI/dV value of Ni/cPPyNP is larger than that of cPPyNP, owing to the intrinsic electrical property of metal nanoparticles. Although the dI/dV values of ND-Ni/cPPyNP are decreased compared with those of Ni/cPPyNP, the ohmic contact endures. The liquid-ion-gate system can achieve more gating effect directly than the back-gate system because of the intimate contact between the transducers and the gate.

Figure 4c displays the $I_{SD}-V_{SD}$ plot of the ND-Ni/cPPyNP electrode for varying V_G. The I_{SD} increases negatively with negatively increasing V_G, meaning the p-type semiconducting behavior of the transducer materials. This was caused by an increase in the oxidation level of the polymer chains.

To demonstrate the advanced performance of NBN, including the sensitivity, selectivity, and stability, we also fabricated Ni/cPPyNP-FET conjugated with TAAR13c in detergent micelle (Mi) that was constructed without the scaffolding lipids with MSP. The Mi was constructed by following our previous studies.[15] The Mi-Ni/cPPyNP-FET was fabricated by the same process as the ND-Ni/cPPyNP-FET. The Ni/cPPyNP and the Mi-Ni/cPPyNP immobilized electrode shows a similar tendency with ND-Ni/cPPyNP, as shown in Figure S2. To investigate the liquid and gas sensing profile, The NBN was intensively fabricated. The normal ratio of fabricated NBN was about 40%. Figure 4d shows the real-time response of ND- and Mi-based biosensors to various concentrations of CV. Here, while adding various concentrations of target solutions, drain-source currents of the sensor were measured using a semiconductor analyzer. The current changes during the additions of CV were normalized by the original current values to estimate the normalized conductance change $\Delta I/I_0$. Note that after adding various concentrations of CV solutions, the conductance of the biosensor was sharply increased. When the CV molecule combines with TAAR13c, the protonated positively charged CV molecule increases the work function of the electrodes. Therefore, the binding of CV on the sensing transducer decreases the Schotty barrier for hole carriers and increases the electrical current in the sensor device. As a result, the resistance of sensor is decreased by the

DOI: 10.1021/acs.analchem.9b01068
Anal. Chem. 2019, 91, 12181−12190

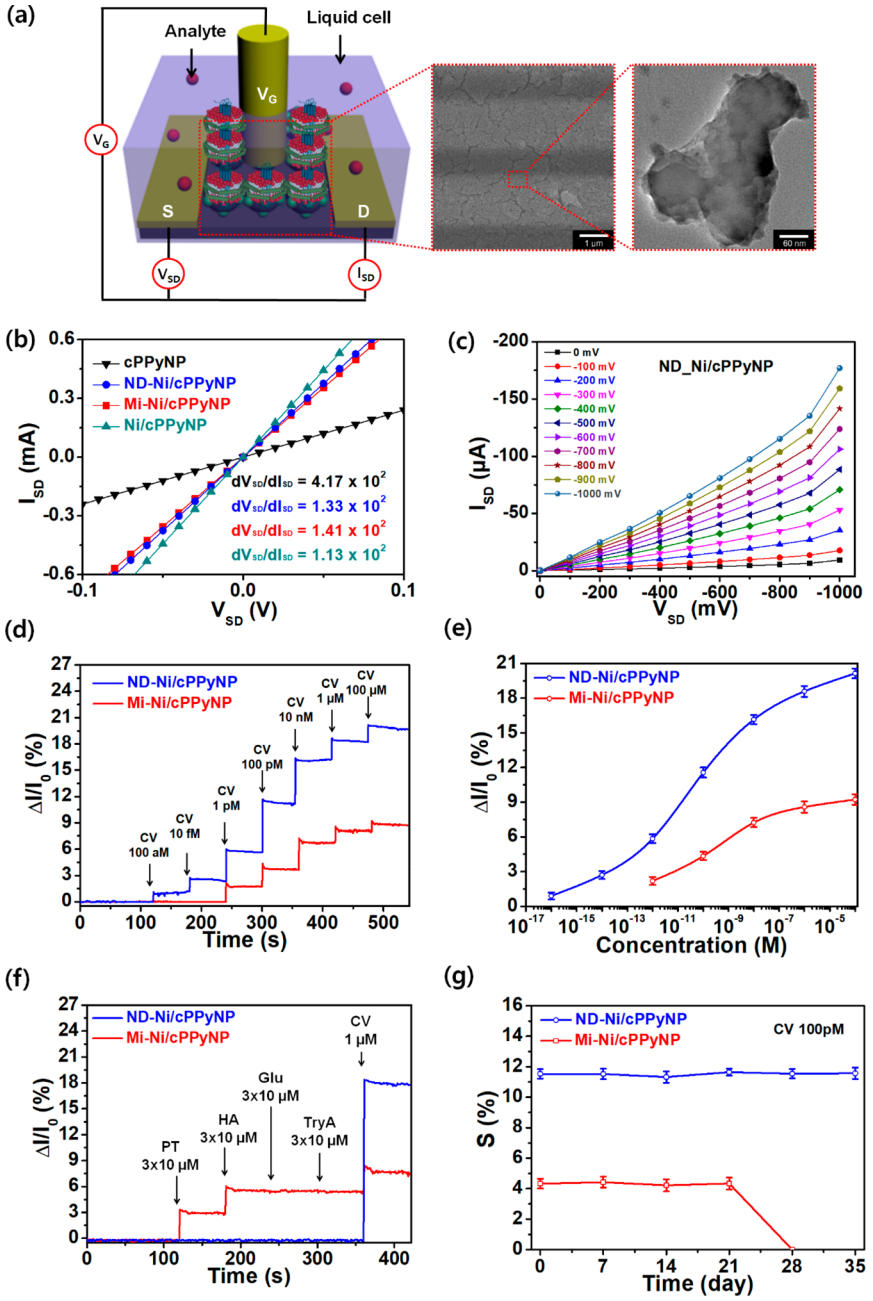

Figure 4. (a) Schematic of the liquid-ion-gate FET sensor electrode and SEM images of ND-Ni/cPPyNP. (b) Source−drain current−voltage (I_{SD}−V_{SD}) curves of FETs with different transducer nanomaterials at V_G = 0. (c) Source−drain current−voltage (I_{SD}−V_{SD}) curves of ND-Ni/cPPyNP for variable gate voltages (V_G) ranging from 0 to 1000 mV in 100 mV steps. (d) Real-time responses of the ND-Ni/cPPyNP and Mi-Ni/cPPyNP to various CV concentrations comprising the effects of receptor structures, with normalized current changes ($(\Delta I/I_0 = (I - I_0)/I_0$), where I_0 is the initial current and I is the instantaneous current). (e) Calibration curves of sensors comprising the saturation concentration of each receptor (n = 3). (f) Real-time responses of CV biosensors with different receptor structures to target (cadaverine (CV)) and nontarget (putrescine (PT), hydroxylamine (HA), glutamine (Glu), tryptamine (TryA)) analytes. (g) Sensing performance of various CV sensors at one-week intervals over 5 weeks (n = 3).

complex of CV and T13ND.[34,37,38] The Mi-based sensor increased conductance by CV solutions with a concentration as low as 1 pM, indicating the high sensitivity of our device. Interestingly, the ND-based biosensor responded to CV with 10^4 times better sensitivity compared to Mi-based sensor. These results clearly demonstrate that the ND was more stable and elaborate, which leads to effective charge transfer; thus, the ND-based device can be an ultrasensitive platform. Moreover, the limit of detection (LOD) of ND-based sensor is about 100 aM, which is much lower than the ND-based bioelectronics nose reported by our previous study, and that of the tolerance of CV in various foods.[18] Therefore, this platform could be practically used in the assessment of food quality. In addition, no study using protein-based sensor has reported the LOD about 100 aM. This indicated that a highly stable ND-based FET sensor can be a powerful tool for detecting the target molecules at very low concentrations. To compare the performances of the biosensing systems, the most efficient method is to estimate the K value assuming a small molecule, because the Langmuir isotherm model, which is related to the

DOI: 10.1021/acs.analchem.9b01068
Anal. Chem. 2019, 91, 12181−12190

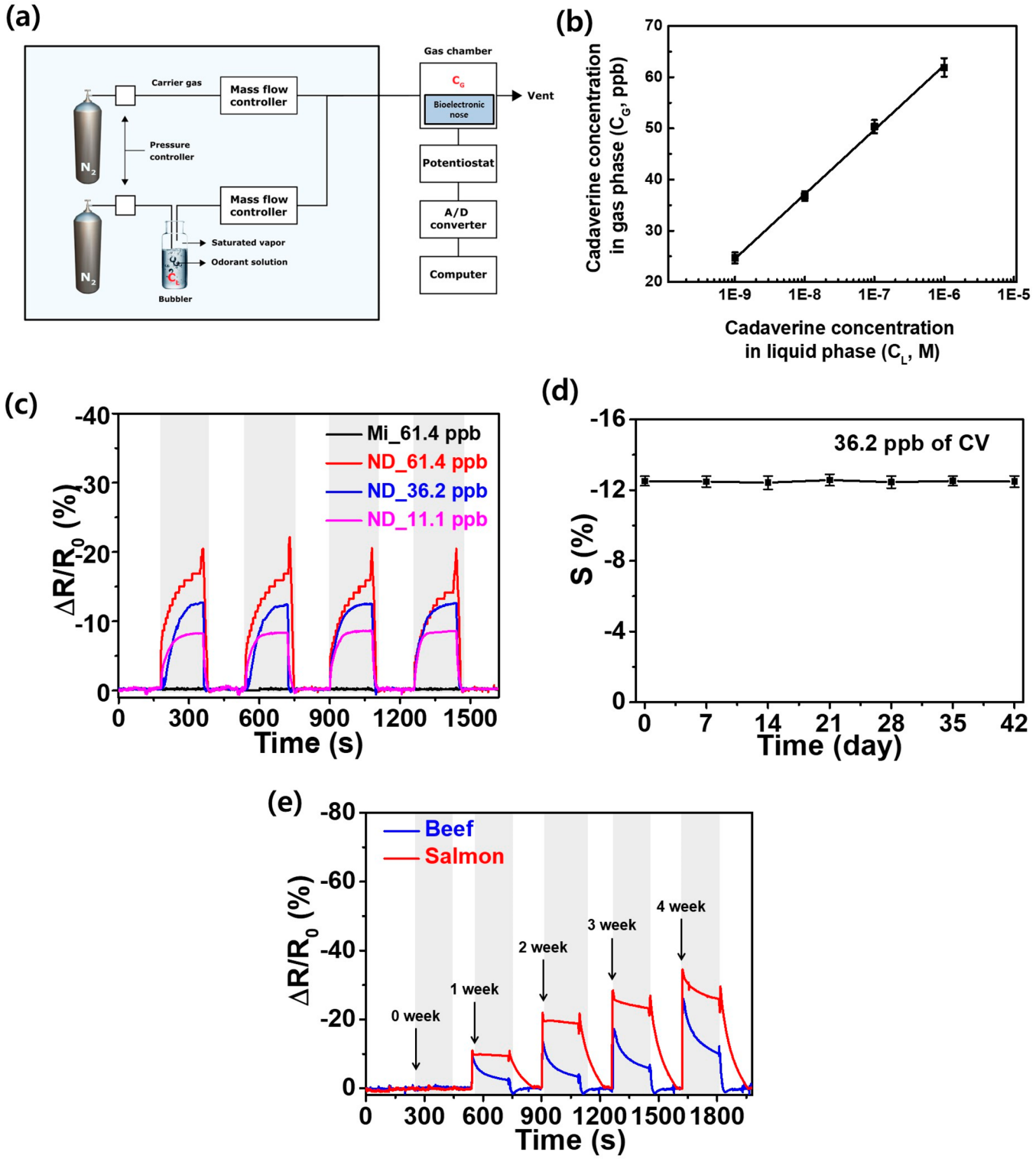

Figure 5. (a) Mimetic diagram of the gas generation system to put CV molecules out to the gas phase. The concentration of CV concentration in gas phase (C_G) was regulated by adjusting the CV concentration in the liquid phase (C_L). (b) Calibration curve of CV concentration in the gas phase (C_G) vs CV concentration in the liquid phase (C_L). (c) Real-time responses of ND-Ni/cPPyNP and Mi-Ni/cPPyNP to various CV concentrations in the gas phase sensing test. (d) Stability test for the ND-Ni/cPPyNP attached sensor platform (n = 3). (e) Real-time responses of the biosensor platforms to the real sample.

equilibrium between analyte molecules and binding sites, enables prediction of their response characteristics. In previous work, K was found using the adsorption and desorption of an olfactory receptor and a small analyte.[13] As a benchmark for the process, K is characterized by the following equation:

$$N = \frac{C}{1/k + C}$$

K can be calculated from the ligand concentrations (C) in the solution and the normalized sensitivity (N), which is the same

DOI: 10.1021/acs.analchem.9b01068
Anal. Chem. 2019, 91, 12181−12190

as the $\Delta I/I_0$ values in Figure 4d. Each K value was calculated based on the dose-dependent curves for each of devices shown in Figure 4e. The K between T13NDs or Mi and CV was (6.253×10^9 and 2.375×10^{10}) M^{-1}, respectively. This result implies that the device can detect target CV molecules with much higher sensitivity than cells or biological systems. Moreover, these results demonstrate that this platform could show reproducible signals in repeated experiments.

Figure 4f shows the real-time responses of the ND- and Mi-based biosensors to various molecules containing amine functional groups. Figure S3 shows the chemical structures of CV and other amines, putrescine (PT), hydroxylamine (HA), glutamine (Glu), and tryptamine (TryA), used in this study. Here, the real-time responses of the sensors were monitored upon the addition of PT, HA, Glu, TryA, and CV in series. PT has a similar structure to CV, HA is monoamine, Glu is an amino acid, and TryA is a derivative of tryptophan. Note that the ND-based device exhibited negligible sensor responses to nontarget molecules, even at a relatively high concentration of 30 μM. However, the conductance of the NBN increased sharply by adding CV at a concentration of 1 μM, which is 30× lower concentration than that of nontarget molecular species; whereas the Mi-based sensor exhibited a nonspecific signal to PT and slightly to HA. This result clearly shows that the ND-based device can selectively detect CV at a very low concentration, even in the presence of high concentrations of similar molecular species. These results clearly demonstrate that the ND-based sensor offers better property in the selectivity for the detection of CV compared to the Mi-based sensor, since the NDs allow the cell membrane-like environment using lipid bilayer and MSP, which efficiently leads to mimicking the binding pocket of natural receptor.

To investigate the stability of receptor-based devices in the liquid-phase, the ND- and Mi-based sensors were stored for 35 days at 4 °C, and their activities to CV were measured every 7 days. Figure 4g shows the stability of the ND- and Mi-based bioelectronic noses. The ND-based device maintained the sensitivity to CV for more than 5 weeks, whereas the activity of Mi-the based device was significantly decreased after 3 weeks. These results clearly indicate the ND-based sensor is much more stable than the Mi-based device. In addition, the stability of ND-based sensor over 5 weeks supported that it can be utilized a practical tool for the development of the protein-based bioelectronic nose with high stability in liquid-phase.

Detection of Gaseous Cadaverine Using the Nanodisc-Based Bioelectronic Nose. To investigate the capability of NBN for the detection of gaseous target, the devices based on ND-Ni/cPPyNP and Mi-Ni/cPPyNP were exposed to gaseous CV. Figure 5a shows a schematic of the gas generation system and its measurement using the bioelectronic noses. The real-time resistance difference was measured as a function of odorant concentration in a nitrogen stream to assess the sensing performance of the Mi- and ND-based biosensors. The concentration of gaseous CV was controlled by the dilution using dimethyl sulfoxside (DMSO) and water. Before gaseous CV detection test, DMSO and water detection test was processed with ND-Ni/cPPyNP based sensing device to prove that the sensing transducer and receptor do not react to solvent of CV. As a result, the sensing device never responds to DMSO or water as analyte despite of high concentration (Figure S4). To measure certain CV gas concentrations from the bubbler outlet, CV gas was collected in a Tedlar bag through the bubbler outlet and analyzed by gas chromatography (G_C) instrument (Figure S5). Diverse CV solutions with low concentrations were used to discover the relation between the liquid (C_L) and gas phase CV samples (C_G), and the linear trend line was suggested as shown in Figure 5b. As a result, 10^{-6}, 10^{-8}, and 10^{-10} M CV solutions (C_L) were estimated as 61.4, 36.2, and 11.1 ppb CV gas (C_G) through the outlet of the bubbler, respectively. Figure 5c represents the real-time responses of the Mi- and ND-based sensors upon periodic exposure to CV gas. A rapid response in resistance was observed from the ND based on the gaseous CV with the minimum detectable level (MDL) of about 10 ppb. However, the Mi-based sensor exhibited no meaningful responses to gaseous CV. The detergent micelles should be disturbed in dried conditions, and the secondary structure of the receptor can be destroyed. On the other hand, the NDs offered an efficient environment for maintaining the active protein structure of receptors, even in dried conditions; thus, the NDs allow a great advantage in detecting the gaseous target with the receptors. In addition, the increased signals of NBNs with gaseous CV were rapidly decreased by flushing with nitrogen gas. The response and restoration times of the device are arranged in the Supporting Information (Table S1). As a result, there is no difference in response time of sensor by CV concentration because the combination of receptors and analytes occurs simultaneously. On the other hand, the restoration time of the sensor increases with increments of CV concentration. Since more receptors combine with increased CV concentration, more time is needed to dissociate analytes from the receptors. After the recovery of signals to the base lines, the reproducible signals were measured by the repeated exposure of CV gas. These results demonstrate that the NBN device allows reversible and reproducible detection of gaseous CV with efficient reusability.

Figure 5d indicates the result from the stability test of the NBN. The responses in resistance of NBN device upon the exposure to CV (36.2 ppb) were measured every week. There was no significant change in the normalized signal intensity over 6 weeks. This clearly indicates the ND-based sensor could be reusable for 6 weeks and offers excellent performance with high stability in the gaseous phase. The enormous sensitivity and stability of NBN in both dried and wet environments are attributed to the fact that the highly stable biomolecule was conjugated with conducting polymer-based nanomaterials, which is not shown in previous reports. These results significantly implied that the conjugation of the biomolecule and the nanomaterial that have environmental stability can have great advantages in sensitivity, selectivity, reproducibility, and stability for the development of a bioelectronic sensor.

Figure 5e shows the real-time responses of the NBNs to various gas samples obtained from spoiled beef and salmon. The beef and salmon were spoiled for 4 weeks, and the gas samples were prepared every week. The NBNs were progressively exposed to 0 to 4 week spoiled gas samples, and the gas chamber was flushed by nitrogen gas after each measurement. The NBNs showed immediate responses to gas samples from spoiled beef and salmon, whereas there was no significant change in signal intensity upon exposure to gas samples obtained from fresh foods (0 week). In addition, the signal intensities were increased in proportion to the spoilage period for salmon and beef. CV is often generated by the bacterial decarboxylation of amino acids contained in many foods, and therefore, the NBN can discriminate the spoiled food by the selective detection of CV.

DOI: 10.1021/acs.analchem.9b01068
Anal. Chem. 2019, 91, 12181−12190

Biogenic amines, including CV, which can be produced by microbial decarboxylation of amino acids in several foods, are important as indicators for the degree of freshness.[23,39] In addition, CV is known as a death-associated odor and can be an important detection target for the scientific investigation.[18,40] For the practical application, the development of analytical tools providing the detection of biogenic amines in the gas phase with a simple procedure of measurement is required. Although the bioelectronic nose based on NDs integrated when CNT-FET has been demonstrated for the aqueous detection of CV in our previous study, the gaseous detection could not be achieved.[18] In this study, the results clearly demonstrate that the responses of NBN are specific to the spoilage of food, and the NBN device can be used to evaluate the freshness of foods. Furthermore, the gaseous detection should provide a simple detection procedure compared to the aqueous detection methods.

CONCLUSIONS

In conclusion, we have developed the T13ND-conjugated Ni/cPPyNP as an FET-type biosensor suited for the sensing of liquid and gaseous CV and demonstrated its potency to practical applications through real-food detection. The outstanding performances of NDN, including sensitivity, selectivity, and stability, were demonstrated by the comparison with the Mi-based biosensor. This study can be used as an attractive methodology for the receptor-based detection of specific targets. Moreover, our strategy could be a generally applicable ND-based platform for a wide range of GPCR research, especially ligand binding analysis. Furthermore, this may offer a powerful strategy for the development of a practical biosensor that can be used as a gaseous system for various applications, such as environmental monitoring, and early diagnosis of disease.

ASSOCIATED CONTENT

Supporting Information

The Supporting Information is available free of charge on the ACS Publications website at DOI: 10.1021/acs.analchem.9b01068.

Materials and methods and supporting figures (PDF)

AUTHOR INFORMATION

Corresponding Authors

*E-mail: hssong@kist.re.kr
*E-mail: thpark@snu.ac.kr.
*E-mail: jsjang@plaza.snu.ac.kr.

ORCID

Oh Seok Kwon: 0000-0002-5936-244X
Hyun Seok Song: 0000-0002-5104-4033
Tai Hyun Park: 0000-0003-4254-0657
Jyongsik Jang: 0000-0002-0415-802X

Present Address

§Protein Engineering Laboratory, Recombinants Unit, MOGAM Institute for Biomedical Research, Yongin 16924, Republic of Korea.

Author Contributions

‡These authors contributed equally to this work.

Notes

The authors declare no competing financial interest.

ACKNOWLEDGMENTS

This research was supported by the National Research Foundation funded by the Korean government (MSIT; NRF-2018R1A2B3004498). This study was also supported by the KIST Institutional Program (No. 2E29530), a National Research Council of Science and Technology (NST) Grant by the Korea government (MSIP; No. CRC-16-01-KRICT), the Korea Basic Science Institute (D38410), and Korea Institute of Planning and Evaluation for Technology in Food, Agriculture and Forestry (IPET) through the Advanced Production Technology Development Program, funded by the Ministry of Agriculture, Food and Rural Affairs (MAFRA; 318104-3).

REFERENCES

(1) Biju, V. *Chem. Soc. Rev.* **2014**, *43*, 744−764.
(2) Zhang, A.; Lieber, C. M. *Chem. Rev.* **2016**, *116*, 215−257.
(3) Mao, S.; Lu, G.; Yu, K.; Bo, Z.; Chen, J. *Adv. Mater.* **2010**, *22*, 3521−3526.
(4) Kwon, O. S.; Lee, S. H.; Park, S. J.; An, J. H.; Song, H. S.; Kim, T.; Oh, J. H.; Bae, J.; Yoon, H.; Park, T. H.; Jang, J. *Adv. Mater.* **2013**, *25*, 4177−4185.
(5) Kwon, O. S.; Park, S. J.; Hong, J.-Y.; Han, A.-R.; Lee, J. S.; Lee, J. S.; Oh, J. H.; Jang, J. *ACS Nano* **2012**, *6*, 1486−1493.
(6) Dong, X.; Shi, Y.; Huang, W.; Chen, P.; Li, L. J. *Adv. Mater.* **2010**, *22*, 1649−1653.
(7) Huang, Y.; Dong, X.; Shi, Y.; Li, C. M.; Li, L.-J.; Chen, P. *Nanoscale* **2010**, *2*, 1485−1488.
(8) Sarkar, T.; Ashraf, P. M.; Srinives, S.; Mulchandani, A. *Sens. Actuators, B* **2018**, *268*, 115−122.
(9) Dennison, M. J.; Hall, J. M.; Turner, A. P. F. *Analyst* **1996**, *121*, 1769−1773.
(10) Buck, L.; Axel, R. *Cell* **1991**, *65*, 175−187.
(11) Hussain, A.; Saraiva, L. R.; Ferrero, D. M.; Ahuja, G.; Krishna, V. S.; Liberles, S. D.; Korsching, S. I. *Proc. Natl. Acad. Sci. U. S. A.* **2013**, *110*, 19579−19584.
(12) Kwon, O. S.; Ahn, S. R.; Park, S. J.; Song, H. S.; Lee, S. H.; Lee, J. S.; Hong, J.-Y.; Lee, J. S.; You, S. A.; Yoon, H.; Park, T. H.; Jang, J. *ACS Nano* **2012**, *6*, 5549−5558.
(13) Kwon, O. S.; Song, H. S.; Park, S. J.; Lee, S. H.; An, J. H.; Park, J. W.; Yang, H.; Yoon, H.; Bae, J.; Park, T. H.; Jang, J. *Nano Lett.* **2015**, *15*, 6559−6567.
(14) Kwon, O. S.; Song, H. S.; Park, T. H.; Jang, J. *Chem. Rev.* **2019**, *119*, 36−93.
(15) Goldsmith, B. R.; Mitala, J. J.; Josue, J.; Castro, A.; Lerner, M. B.; Bayburt, T. H.; Khamis, S. M.; Jones, R. A.; Brand, J. G.; Sligar, S. G.; Luetje, C. W.; Gelperin, A.; Rhodes, P. A.; Discher, B. M.; Johnson, A. T. C. *ACS Nano* **2011**, *5*, 5408−5416.
(16) Lee, S. H.; Kwon, O. S.; Song, H. S.; Park, S. J.; Sung, J. H.; Jang, J.; Park, T. H. *Biomaterials* **2012**, *33*, 1722−1729.
(17) Kiefer, H.; Krieger, J.; Olszewski, J. D.; Von Heijne, G.; Prestwich, G. D.; Breer, H. *Biochemistry* **1996**, *35*, 16077−16084.
(18) Yang, H.; Kim, D.; Kim, J.; Moon, D.; Song, H. S.; Lee, M.; Hong, S.; Park, T. H. *ACS Nano* **2017**, *11*, 11847−11855.
(19) Jin, H. J.; Lee, S. H.; Kim, T. H.; Park, J.; Song, H. S.; Park, T. H.; Hong, S. *Biosens. Bioelectron.* **2012**, *35*, 335−341.
(20) Lim, J. H.; Park, J.; Oh, E. H.; Ko, H. J.; Hong, S.; Park, T. H. *Adv. Healthcare Mater.* **2014**, *3*, 360−366.
(21) Park, J.; Lim, J. H.; Jin, H. J.; Namgung, S.; Lee, S. H.; Park, T. H.; Hong, S. *Analyst* **2012**, *137*, 3249−3254.
(22) Pinel, J. P.; Gorzalka, B. B.; Ladak, F. *Physiol. Behav.* **1981**, *27* (5), 819−824.
(23) Pacquit, A.; Lau, K. T.; McLaughlin, H.; Frisby, J.; Quilty, B.; Diamond, D. *Talanta* **2006**, *69*, 515−520.
(24) Liu, C.-H. J.; Lu, W.-C. *J. Chin. Inst. Chem. Eng.* **2007**, *38*, 483−488.
(25) Park, E.; Kwon, O. S.; Park, S. J.; Lee, J. S.; You, S.; Jang, J. *J. Mater. Chem.* **2012**, *22*, 1521−1526.

DOI: 10.1021/acs.analchem.9b01068
Anal. Chem. 2019, 91, 12181−12190

(26) Ko, S.; Jang, J. *Biomacromolecules* **2007**, *8*, 182−187.
(27) Lo, Y.-S.; Nam, D. H.; So, H.-M.; Chang, H.; Kim, J.-J.; Kim, Y. H.; Lee, J.-O. *ACS Nano* **2009**, *3*, 3649−3655.
(28) Bonroy, K.; Frederix, F.; Reekmans, G.; Dewolf, E.; De Palma, R.; Borghs, G.; Declerck, P.; Goddeeris, B. *J. Immunol. Methods* **2006**, *312*, 167−181.
(29) Lee, M.; Yang, H.; Kim, D.; Yang, M.; Park, T. H.; Hong, S. *Sci. Rep.* **2018**, *8*, 13945.
(30) Hong, J. Y.; Yoon, H.; Jang, J. *Small* **2010**, *6*, 679−686.
(31) Sarramegna, V.; Talmont, F.; Demange, P.; Milon, A. *Cell. Mol. Life Sci.* **2003**, *60*, 1529−1546.
(32) Kim, T. H.; Song, H. S.; Jin, H. J.; Lee, S. H.; Namgung, S.; Kim, U.-k.; Park, T. H.; Hong, S. *Lab Chip* **2011**, *11*, 2262−2267.
(33) Song, H. S.; Kwon, O. S.; Lee, S. H.; Park, S. J.; Kim, U.-K.; Jang, J.; Park, T. H. *Nano Lett.* **2013**, *13*, 172−178.
(34) Kim, B.; Song, H. S.; Jin, H. J.; Park, E. J.; Lee, S. H.; Lee, B. Y.; Park, T. H.; Hong, S. *Nanotechnology* **2013**, *24*, 285501.
(35) Michalke, K.; Graviere, M.-E.; Huyghe, C.; Vincentelli, R.; Wagner, R.; Pattus, F.; Schroeder, K.; Oschmann, J.; Rudolph, R.; Cambillau, C.; Desmyter, A. *Anal. Biochem.* **2009**, *386*, 147−155.
(36) Park, S. J.; Yang, H.; Lee, S. H.; Song, H. S.; Park, C. S.; Bae, J.; Kwon, O. S.; Park, T. H.; Jang, J. *ACS Nano* **2017**, *11*, 5950−5959.
(37) Sharma, K.; Ahuja, G.; Hussain, A.; Balfanz, S.; Baumann, A.; Korsching, S. I. J. S. r. *Sci. Rep.* **2016**, *6*, 28359.
(38) Kim, B.; Lee, J.; Namgung, S.; Kim, J.; Park, J. Y.; Lee, M.-S.; Hong, S. *Sens. Actuators, B* **2012**, *169*, 182−187.
(39) Önal, A. *Food Chem.* **2007**, *103*, 1475−1486.
(40) Liberles, S. D. *Curr. Opin. Neurobiol.* **2015**, *34*, 1−7.

DOI: 10.1021/acs.analchem.9b01068
Anal. Chem. 2019, 91, 12181−12190